Near infrared-modulated propulsion of catalytic Janus polymer multilayer capsule motors

ARTICLE *in* CHEMICAL COMMUNICATIONS · NOVEMBER 2014

Impact Factor: 6.83 · DOI: 10.1039/c4cc07182d · Source: PubMed

4 AUTHORS, INCLUDING:

Tieyan Si
Harbin Institute of Technology
31 PUBLICATIONS **63** CITATIONS
SEE PROFILE

Xiankun Lin
Harbin Institute of Technology
21 PUBLICATIONS **326** CITATIONS
SEE PROFILE

Qiang He
Harbin Institute of Technology
102 PUBLICATIONS **3,203** CITATIONS
SEE PROFILE

ChemComm

COMMUNICATION

View Article Online
View Journal

Cite this: DOI: 10.1039/c4cc07182d

Received 11th September 2014,
Accepted 12th November 2014

DOI: 10.1039/c4cc07182d

www.rsc.org/chemcomm

Near infrared-modulated propulsion of catalytic Janus polymer multilayer capsule motors†

Yingjie Wu, Tieyan Si, Xiankun Lin* and Qiang He*

The use of a near-infrared (NIR) laser for reversible modulation of a bubble-driven Janus polymer capsule motor is demonstrated. This process was mediated through illumination of the metal face of the Janus capsule motor at the critical concentration of peroxide fuel. Such an effective control of the propulsion of chemically powered microengines holds a considerable promise for diverse applications.

Chemically powered artificial nano/micromachines with autonomous motion have recently attracted considerable interest, owing to their great promise for diverse future applications, such as in nanoscale assembly and transport, microfactories, microactuators, drug delivery, nanoscale surgery, and motion-based biosensing.[1–3] Such challenging applications require new capabilities of chemically catalytic motors, including increased propulsion power, surface functionalization, precise motion control, and efficient cargo loading, transport and release.[4–6] Particularly, a precise control of the motion of such motors as well as the position and duration of time for which the motors work are important for performing various tasks and diverse applications in future.[7–10] Control of the directionality of chemically catalytic nano/micromotors has been commonly achieved by means of an external magnetic field or fuel concentration gradients.[11–16] Also, several strategies have been developed to regulate the speed of the motors, including application of thermal and electrical stimuli as well as ultraviolet or visible light.[17–20] Obviously, a physical input can be conveniently employed to turn on or off the motion in a wide range of environments at will. Moreover, light in the near-infrared (NIR) region is of special interest in the context of biomedical applications because body tissues have the highest transmissivity in this region (the so-called biological window).[21,22]

Here we demonstrate how the NIR-modulated "on/off" motion of a polymer multilayer capsule micromotor coated with a thin platinum (Pt) shell can be achieved in a critical concentration region of peroxide fuel (0.02–0.1%, v/v). Compared to other catalytic nanoengines, the capsule-based motors offer a large space for encapsulating therapeutic payload.[23–27] In the previous studies, it has been found that with the decrease of fuel concentrations, the speed of chemically catalytic micromotors dramatically drops down, but can be enhanced with the increase of the solution temperature. In other words, the movement of such catalytic engines can be modulated by a small change in the localized temperature. The thin Pt shell plays two roles: it acts as a catalyst for the decomposition of the peroxide fuel and as a photothermal agent for heat generation. Upon NIR irradiation on the Pt face of a Janus capsule motor, the absorbed electromagnetic energy is dissipated as heat and thus forms a thermal gradient along the direction from the Pt surface to the surrounding solution. This increased temperature gradient results in the accelerated kinetics of the catalytically chemical process, and the increased rates of mass transport. Therefore, the motion of Janus capsule motors could be modulated at will through a photothermal effect under a NIR laser illumination.

Janus polymer multilayer capsules were fabricated by a template-assisted layer-by-layer (LbL) method according to the procedures previously reported.[28–31] Briefly, five bilayers of negatively charged poly(styrene sulfonate) (PSS) and positively charged poly(allylamine hydrochloride) (PAH) were alternately absorbed on the surface of 8 μm silica particles *via* the LbL assembly. Next, $(PSS/PAH)_5$-coated silica particles were deposited on a glass slide and then a 20 nm Pt layer was sputtered as illustrated in Fig. 1A. Finally, Pt-modified Janus $(PSS/PAH)_5$ capsule motors were obtained after the removal of the silica templates. Scanning electron microscopy (SEM) images in Fig. 1B and C reveal the successful preparation of Janus $(PSS/PAH)_5$ capsule motors before and after the removal of silica templates. The diameter of $(PSS/PAH)_5$ capsule motors is approximately 8 μm corresponding to the size of used silica templates. For details of the deposition, characterization and NIR-irradiation methods see the ESI.† The brighter parts are ascribed to the deposition of the Pt component, and the surface area of the deposited Pt

Key Lab for Microsystems and Microstructure Manufacturing, Micro/Nanotechnology Research Centre, Harbin Institute of Technology, Yi Kuang Jie 2, Harbin 150080, China. E-mail: xiankunlin@hit.edu.cn, qianghe@hit.edu.cn

† Electronic supplementary information (ESI) available: Related experimental protocols instrumentation, reagents, additional data and movies. See DOI: 10.1039/c4cc07182d

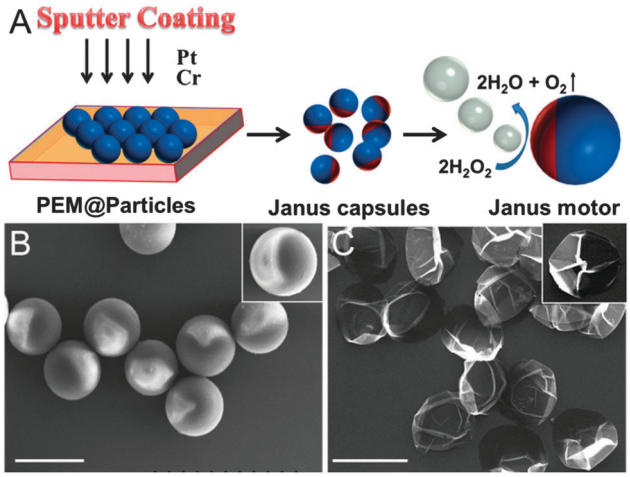

Fig. 1 (A) Scheme of the synthetic procedure of Janus polymer multilayer capsule motors by using the layer-by-layer technique combined with a metal sputtering deposition method. (B, C) SEM images of Janus $(PSS/PAH)_5$ capsule motors before and after removal of the silica templates. Scale bar = 10 μm.

layers is roughly 40–50% of the total surface area of the capsule motors. The corresponding energy-dispersive X-ray (EDX) mapping analysis (ESI,† Fig. S1) displays the asymmetric distribution of Pt layers on Janus $(PSS/PAH)_5$ capsule motors. After the $(PSS/PAH)_5$ shells were labelled using a fluorescent isothiocyanate (FITC) dye, both fluorescence microscopy and confocal laser scanning microscopy images (ESI,† Fig. S2) show a green Janus structure, confirming the formation of Janus capsule motors and the stability of the assembled PSS/PAH multilayers.

As illustrated in Fig. 2A, optical microscopy images, taken from the ESI,† Video 1, show the bubble-driven movement of Janus $(PAH/PSS)_5$ capsule motors in hydrogen peroxide (H_2O_2) at concentrations of 1%, 2%, 3%, and 5%, respectively. One can see that all of the oxygen bubbles were generated and subsequently released from the dark side (*i.e.* Pt layer), showing that Janus $(PAH/PSS)_5$ capsule motors are propelled unidirectionally by the generated oxygen bubbles. Also, a tail of oxygen bubbles could be observed at 5% H_2O_2, showing that the frequency of oxygen bubble release is higher than that at other lower fuel concentrations. This means that the speed at 5% H_2O_2 is higher than others because the higher frequency of oxygen bubble release corresponds to the higher speed of Janus capsule motors. The inset red lines represent the tracking trajectories of Janus $(PAH/PSS)_5$ capsule motors in one second accordingly. One can see that the motor at 5% H_2O_2 could travel the longest distance compared with those at 1%, 2% and 3%, respectively. Furthermore, Fig. 2B demonstrates that the speed of Janus $(PAH/PSS)_5$ capsule motors goes up with the increase of fuel concentrations. The average speed of the capsule motors increases from roughly 2 μm s^{-1} at 0.5% H_2O_2 to the maximum speed of about 140 μm s^{-1} at 5% H_2O_2 (18 body lengths s^{-1}) (Fig. 2B left *y*-axis, red line). It was found that with the decrease of peroxide fuel concentrations, the percentage of the activated catalytic micromotors dramatically drops from 85% at 5% H_2O_2 down to 10% at 0.5% H_2O_2 (Fig. 2B right *y*-axis, black line) accordingly. Obviously, all Janus $(PAH/PSS)_5$ capsule motors are almost

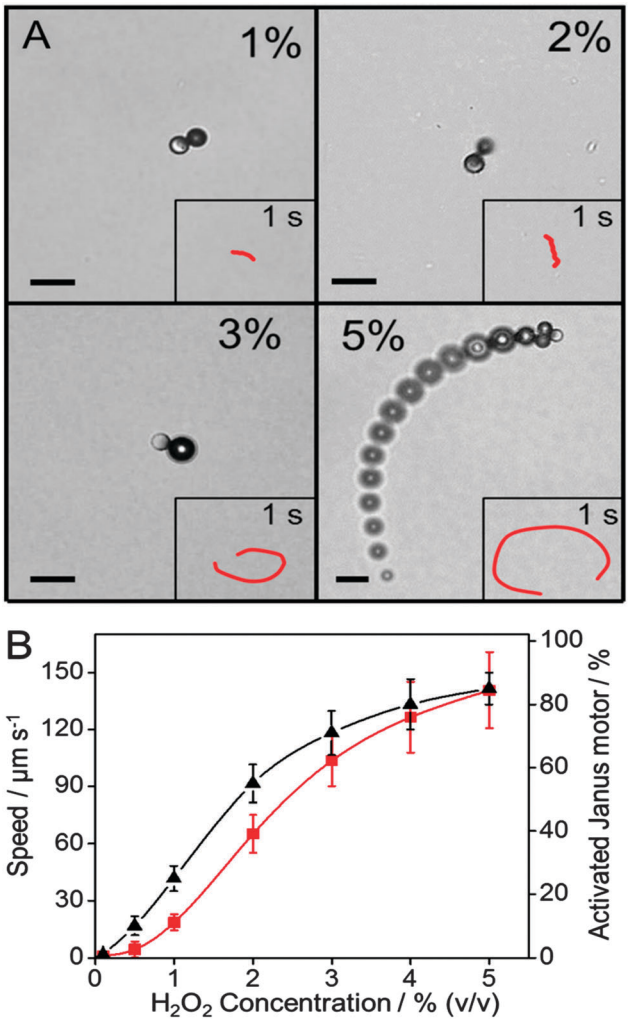

Fig. 2 (A) The optical microscopic images of the self-propulsion of Janus $(PAH/PSS)_5$ capsule motors in 1%, 2%, 3%, and 5% H_2O_2, respectively. The inset red curves represent the trajectories of Janus motors in 1 s. Scale bar = 10 μm. (B) Both the average speed (red curve) and the activated percentage (black curve) of catalytic Janus $(PAH/PSS)_5$ capsule motors change with the peroxide concentrations.

motionless below 0.5% H_2O_2, which may be regarded as a critical fuel concentration region for effectively propelling Janus capsule motors.

Fig. 3A shows that three Janus $(PAH/PSS)_5$ capsule motors remain motionless at 0.1% H_2O_2 at room temperature. In order to better understand the local photothermal effect on the "on/off" motion, two close Janus $(PAH/PSS)_5$ capsule motors were taken as a reference and a focused NIR laser at 808 nm with a power of 3 mW μm^{-2} was employed to illuminate that single capsule motor. The laser irradiation setup was home-made. We have described the setup in the ESI,† Fig. S3. Before exposure to the NIR laser, the Janus $(PAH/PSS)_5$ capsule motor stays in the "motion off" state. Once irradiated by the NIR laser, the light-activated micromotor was accelerated within 0.3 s (a "motion on" state) and then reached to the maximum speed of 220 μm s^{-1} compared to the referenced capsules, as shown in Fig. 3A and ESI,† Video 2. It can be seen that once a NIR-activated

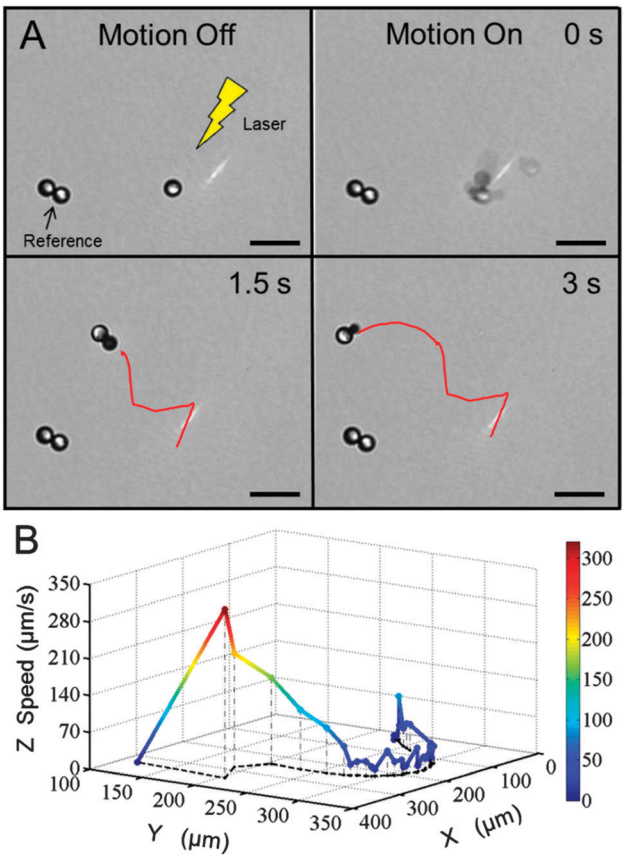

Fig. 3 (A) The time-lapse optical microscopic images of the "switch on" motion of a Janus $(PAH/PSS)_5$ capsule motor under a focused NIR laser irradiation at 0.1% H_2O_2. The red line represents the tracking trajectory. (B) 3D profiles of the coloured curve correspond to the trajectories (*x*, *y*) and the speed (*z*) of the motion in (A). Scale bar = 20 μm.

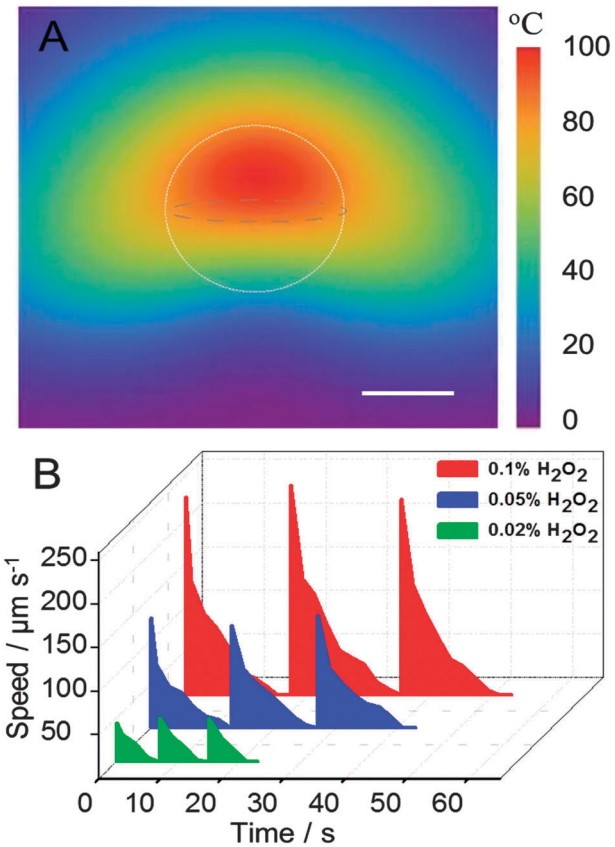

Fig. 4 (A) Simulation of the photothermal effect of a micromotor. The elevated profile of temperature distribution on the vertical cross-section of a Janus motor irradiated with a laser power of 3 mW μm^{-2}. Scale bar = 5 μm. (B) Cyclic "On" and "Off" laser activation of the microengine motion. Data shown represent the average speed of motors in 0.02%, 0.05%, and 0.1% H_2O_2, respectively.

microengine starts to move, it leaves the focused area of the NIR laser and then the speed of the microengine gradually decreases to 0 μm s^{-1} in 17 s. The NIR-activated movement of the Janus capsule motor is ascribed to the fact that NIR irradiation on the Pt side leads to the local increase of temperature surrounding the microengines because metals are known to dissipate heat upon light absorption. Therefore, the sharp increase of temperature rapidly induces higher rates of catalytic decomposition and mass transport, producing more bubbles and stronger propulsion force accordingly. The component of the bubbles was monitored by gas chromatography-mass spectrometry. The results indicate that the generated bubbles consist of oxygen, and no other gas components were detected (ESI,† Fig. S4). Moreover, the residual heat could still maintain a higher temperature so that the catalytic decomposition of the peroxide fuel continues to occur even though the engine has left the laser spot.

To better understand the photothermal effect of Janus capsule motors under NIR irradiation, we simulated the temperature change by using a heat diffusion equation that was used to study the thermoplasmonics modelling of Janus particles.[32] When irradiated with the NIR laser, the Janus motor creates a local "hot spot" in the centre of the metal shell, causing the temperature to soar above 100 °C within less than one second. Due to the heat diffusion, a temperature gradient along the direction from the Pt surface to the surrounding solution is formed, and the corresponding temperature profiles shown in Fig. 4A were obtained by solving the heat diffusion equation. According to our simulation, the rapid decay of temperature at the Pt/water interface also contributes to the initial acceleration due to the Soret effect. Compared to the bubble propulsion, however, this contribution could be neglected because the temperature difference is low and only lasts a short time in our study. In the control experiment, the start-up did not occur for the Janus motor in H_2O after NIR laser irradiation (ESI,† Fig. S5 and Video 4). These results suggest that the contribution of scattering and radiation pressure of the NIR laser or thermophoresis is also faint.

Reversibly stopping and starting the propulsion of catalytic Janus $(PAH/PSS)_5$ capsule motors should be performed by using this method. Fig. 4B and the corresponding ESI,† Video 3, display the reversible "on/off" switching of the motion of Janus $(PAH/PSS)_5$ capsule motors at the peroxide fuel concentrations of 0.02% (a), 0.05% (b), and 0.1% (c). Similarly, Janus $(PAH/PSS)_5$ capsule motors remain motionless before switching on the laser. However, a sharp increase of the velocity is observed

upon application of NIR illumination within 0.3 s. The maximum average speeds of the microengines are 45 ± 10, 120 ± 20, and 230 ± 30 μm s^{-1} in the presence of 0.02%, 0.05%, and 0.1% H_2O_2, respectively. When the capsule motors left the focused region of the NIR laser which is regarded as switching off the NIR laser, the microengine motion stopped slowly in the 0.02%, 0.05%, and 0.1% H_2O_2 after 7, 13, and 17 s, respectively. These results further demonstrate that the maximum speeds of catalytic Janus capsule motors are also dependent on different fuel levels. Therefore, a wide range of micromotor speeds and run durations could be modulated through a combination of the fuel concentration and NIR illumination.

The rapidly starting artificial capsule motor is attributed to the accelerated kinetics of both the oxidation and reduction reactions of the peroxide fuel, and to a lower solution viscosity (and hence diminished resistance) with the rising local temperature. At higher temperature, the increasing molecular motion around the metallic shell also leads to the improved rates of mass transport, so that the fuel consumption can be supplemented quickly. In this case, the photothermal effect caused by laser irradiation could lower the threshold of chemical fuel concentrations to propel Janus motors. However, when the motors moved out of the laser-illuminated region, the photothermal effect disappeared. As a result, the temperature of the metal shell started to drop to room temperature and thus led to the deceleration of the micromotors.

In conclusion, we have demonstrated a novel approach for instantaneous activation of the motion of Janus catalytic motors by the remote NIR stimuli at the critical concentration of the peroxide fuel. Such rapid and reversible motion control is attributed to the fact that a local sharp increase of temperature around the micromotors due to a NIR-based photothermal effect results in the accelerated kinetics of redox processes and increased rates of mass transport. The ''on/off'' switching of the motion of Janus capsule motors can be repeated many times by using an external ''on/off'' NIR laser switch. The NIR-triggered speed modulation capability can be expanded to other types of chemically catalytic motors and thus paves the way to apply self-propelled synthetic engines in future.

This work was supported by the National Nature Science Foundation of China (91027045), and the Fundamental Research Funds for the Central Universities.

Notes and references

1 W. Gao and J. Wang, *ACS Nano*, 2014, **8**, 3170–3180.
2 Y. Mei, A. A. Solovev, S. Sanchez and O. G. Schmidt, *Chem. Soc. Rev.*, 2011, **40**, 2109–2119.
3 W. Gao, A. Pei and J. Wang, *ACS Nano*, 2012, **6**, 8432–8438.
4 F. Z. Mou, C. R. Chen, H. R. Ma, Y. X. Yin, Q. Z. Wu and J. G. Guan, *Angew. Chem., Int. Ed.*, 2013, **52**, 7208–7212.
5 R. F. Ismagilov, A. Schwartz, N. Bowden and G. M. Whitesides, *Angew. Chem., Int. Ed.*, 2002, **41**, 652–654.
6 M. Pumera, *Nanoscale*, 2010, **2**, 1643–1649.
7 J. Gibbs and Y. Zhao, *Frontiers of Materials Science*, 2011, **5**, 25–39.
8 J. Wang and K. M. Manesh, *Small*, 2010, **6**, 338–345.
9 S. Sanchez, A. N. Ananth, V. M. Fomin, M. Viehrig and O. G. Schmidt, *J. Am. Chem. Soc.*, 2011, **133**, 14860–14863.
10 Z. Wu, X. Lin, Y. Wu, T. Si, J. Sun and Q. He, *ACS Nano*, 2014, **8**, 6097–6105.
11 S. Balasubramanian, D. Kagan, K. M. Manesh, P. Calvo-Marzal, G. U. Flechsig and J. Wang, *Small*, 2009, **5**, 1569–1574.
12 M. Xuan, J. Shao, X. Lin, L. Dai and Q. He, *ChemPhysChem*, 2014, **15**, 2255–2260.
13 D. A. Wilson, R. J. M. Nolte and J. C. M. van Hest, *Nat. Chem.*, 2012, **4**, 268–274.
14 V. Magdanz, G. Stoychev, L. Ionov, S. Sanchez and O. G. Schmidt, *Angew. Chem., Int. Ed.*, 2014, **53**, 2673–2677.
15 W. Gao, A. Pei, X. Feng, C. Hennessy and J. Wang, *J. Am. Chem. Soc.*, 2013, **135**, 998–1001.
16 Z. Wu, Y. Wu, W. He, X. Lin, J. Sun and Q. He, *Angew. Chem., Int. Ed.*, 2013, **52**, 7000–7003.
17 V. Yadav, H. Zhang, R. Pavlick and A. Sen, *J. Am. Chem. Soc.*, 2012, **134**, 15688–15691.
18 A. A. Solovev, E. J. Smith, C. C. Bof'Bufon, S. Sanchez and O. G. Schmidt, *Angew. Chem., Int. Ed.*, 2011, **50**, 10875–10878.
19 T. Xu, F. Soto, W. Gao, V. Garcia-Gradilla, J. Li, X. Zhang and J. Wang, *J. Am. Chem. Soc.*, 2014, **136**, 8552–8555.
20 Z. Liu, J. Li, J. Wang, G. Huang, R. Liu and Y. Mei, *Nanoscale*, 2013, **5**, 1345–1352.
21 F. Z. Mou, C. R. Chen, Q. Zhong, Y. X. Yin, H. R. Ma and J. G. Guan, *ACS Appl. Mater. Interfaces*, 2014, **6**, 9897–9903.
22 L. Xu, H. Kuang, C. Xu, W. Ma, L. Wang and N. A. Kotov, *J. Am. Chem. Soc.*, 2012, **134**, 1699–1709.
23 E. Donath, G. B. Sukhorukov, F. Caruso, S. A. Davis and H. Möhwald, *Angew. Chem., Int. Ed.*, 1998, **37**, 2201–2205.
24 M. Delcea, H. Mohwald and A. G. Skirtach, *Adv. Drug Delivery Rev.*, 2011, **63**, 730–747.
25 J. Zhao, J. Fei, L. Gao, W. Cui, Y. Yang, A. Wang and J. Li, *Chem. – Eur. J.*, 2013, **19**, 4548–4555.
26 K. Ariga, Y. M. Lvov, K. Kawakami, Q. Ji and J. P. Hill, *Adv. Drug Delivery Rev.*, 2011, **63**, 762–771.
27 F. Caruso, *Chem. – Eur. J.*, 2000, **6**, 413–419.
28 X. Yan, J. Li and H. Mohwald, *Adv. Mater.*, 2012, **24**, 2663–2667.
29 D. Volodkin, A. Skirtach and H. Mohwald, *Polym. Int.*, 2012, **61**, 673–679.
30 Y. Wu, Z. Wu, X. Lin, Q. He and J. Li, *ACS Nano*, 2012, **6**, 10910–10916.
31 Y. Jia, Y. Cui, J. B. Fei, M. C. Du, L. R. Dai, J. B. Li and Y. Yang, *Adv. Funct. Mater.*, 2012, **22**, 1446–1453.
32 M. Z. Zhang, R.-N. Yu, J. Chen, Z.-Y. Ma and Y.-D. Zhao, *Nanotechnology*, 2012, **23**, 485104.

